

Exotic d-wave Bose Metal in two dimensions

Zhangkai Cao,^{1,*} Jiahao Su,^{1,2,*} Jianyu Li,^{1,2} Tao Ying,³ WanSheng Wang,^{4,†} Jin-Hua Sun^{*,4,‡} Ho-Kin Tang,^{1,2,§} and Haiqing Lin⁵

¹*School of Science, Harbin Institute of Technology, Shenzhen, 518055, China*

²*Shenzhen Key Laboratory of Advanced Functional Carbon Materials
Research and Comprehensive Application, Shenzhen 518055, China.*

³*School of Physics, Harbin Institute of Technology, Harbin 150001, China*

⁴*Department of Physics, Ningbo University, Ningbo 315211, China*

⁵*Institute for Advanced Study in Physics and School of Physics, Zhejiang University, Hangzhou, 310058, China.*

(Dated: May 27, 2024)

The Landau Fermi liquid theory, a cornerstone in condensed matter physics, encounters limitations in explaining certain phenomena, like the peculiar behavior of strange metals in high-temperature superconductors. Non-Fermi liquids, like Bose metals with uncondensed bosonic ground state, offer potential explanations, yet constructing an elusive Bose metal phase in two dimensions (2D) remains a formidable challenge. Utilizing constraint path quantum Monte Carlo and functional renormalization group methods on a fermionic system with spin anisotropy in a 2D lattice, we reveal the emergence of a Cooper pair Bose metal in a highly anisotropic regime ($\alpha < 0.30$) with wide range of filling, most notably at a filling fraction of $n \sim 0.8$. Our findings exhibit a visible nonzero momentum Bose surface in the Cooper-pair distribution function, accompanied by a distinct signal of d_{xy} correlation between pairs. Our results highlight that spin-dependent anisotropy in the Fermi surface leads to versatile pairing forms. Platforms such as ultracold atoms in optical lattices and recently proposed altermagnets hold promise for realizing this intriguing phase.

In the almost four decades since the discovery of high-temperature (T_c) cuprate superconductors [1], significant progress has been made in understanding the novel quantum properties exhibited by strongly correlated electron systems, many of which defy Landau's Fermi-liquid theory [2]. Among these phenomena, the astonishing complexity of the phase diagram, particularly the strange metal behavior observed in the pseudogap region, has not yet been explained by a plausible non-Fermi liquid theory, which has always been a persistent and significant challenge in condensed matter physics [3–5]. No theoretical consensus has been reached about the origin of high T_c superconductivity. One of the most reputed try is the resonating valence bond (RVB) state proposed by Anderson, in which the spins form a superposition of singlets in cuprate [6]. The charge and spin degrees of freedom are thus separated, and it is argued that electron pairings are mediated by spin fluctuations, resulting in unconventional superconductivity [7].

Unlike conventional metals, we need a gapless and compressible non-Fermi liquid phase to explain the experimental observation in strange metals [8]. Spin liquid and Bose liquid are two good candidates. A spin liquid is a state of matter in which the spins are disordered and highly entangled [9]. There is a belief that doping the spin liquid naturally leads to the emergence of the d -wave superconducting state. Beyond one dimension (1D), a number of interesting candidate materials has emerged

through some circumstantial evidence that might host quantum spin liquids[10]. On the other hand, Bose liquid presumes that Cooper pairs are dominant charge carriers for the electric transport not only in the superconducting but also in the metallic phases, constitute a conducting quantum fluid instead of a superfluid [11]. The existence of a Bose liquid phase could potentially address the obstacle that has hindered the slave-particle gauge theory from explaining the strange metal phase for over 30 years [12].

The two-dimensional (2D) Bose liquid is argued to leave fingerprint in a microscopic lattice model of hardcore bosons with ring exchange on multileg ladders, which called bosonic $J - K$ model [13, 14]. With density matrix renormalization group (DMRG) and variational Monte Carlo (VMC) methods, Bose liquid is argued to leave fingerprint in these ladders model. Gluing these non-trivial bosonic degree of freedom with fermionic spinon, physical electrons emerge, governed by the spin-singlet t - J - K model Hamiltonian, revealing a d -wave Bose metal (DBM) phase as the quantum ground state in ladder models [15]. Prohibiting double occupancy, the relevant energy scales of the ring term K can be comparable to effective hopping term t and antiferromagnetic spin exchange couplings term J (See method for connection with cuprates). They find evidence for the fingerprint of DBM phase in two-leg ladder, however, how 2D DBM would appear is still unanswered.

As another line of attacking the problem, Cooper pair Bose metal (CPBM) has been theoretically proposed to exist in 2D systems with no polarization [16, 17]. The Cooper pairs would form a collective state with gapless excitations along a Bose surface but no condensate in momentum space. The anisotropic spin-dependent Fermi

* These authors contributed equally.

† wangwansheng@nbu.edu.cn

‡ sunjinhua@nbu.edu.cn

§ denghaojian@hit.edu.cn

surface plus attractive interactions leads to an effective model of Cooper pairs with a ring-exchange term, that may allow to realize a paired but non-superfluid Bose metal phase. The attraction here originates from the gauge interaction between the fermionic partons, resulting in bosonic chargon in the slave-particle gauge theory. Notably, they find the fingerprint of Bose metal phase in the two-leg ladder [17] and the four-leg triangular ladder [18], respectively. However, similar to the boson $J - K$ model, the studies are restricted to quasi-1D system due to the method constraint. The full 2D studies of possible Bose liquid still wait to be uncovered.

In this manuscript, we investigate the evolution of exotic phases in an attractive interacting fermionic system with hopping anisotropy between two species of spins in full 2D lattice, utilizing the constrained path quantum Monte Carlo (CPQMC) [19] and the functional renormalization group (FRG) [20]. We found the CPBM phase in 2D system, in which fermions are paired as bosons, and the uncondensed Cooper pairs form a non-superfluid Bose metal, emerging when a spin-dependent anisotropy suppresses the ordinary s -wave superfluid (s-SF). The dominant d -wave nature of Cooper pair correlation is also observed. With varying filling and anisotropy, other phases like charge density wave (CDW) near half filling and incommensurate density wave (IDW) at other fillings are also found.

The Hamiltonian of Hubbard model on a square lattice given by

$$H = - \sum_{i,\sigma,l=\hat{x},\hat{y}} \left(t_{l,\sigma} c_{i,\sigma}^\dagger c_{i+l,\sigma} + h.c. \right) + U \sum_i n_{i,\uparrow} n_{i,\downarrow} \quad (1)$$

with spin-dependent anisotropic hopping amplitudes $t_{l,\sigma}$, on-site attraction interaction $U < 0$, $c_{i,\sigma}^\dagger$ ($c_{i,\sigma}$) creation (annihilation) operators with spin $\sigma = \uparrow, \downarrow$, and $n_{i,\sigma} = c_{i,\sigma}^\dagger c_{i,\sigma}$. For defining the anisotropy of fermion hopping, we define a variable α , where $t_{\hat{y}\downarrow} = t_{\hat{x}\uparrow} = t$, $t_{\hat{x}\downarrow} = t_{\hat{y}\uparrow} = \alpha t$ (we assume $t = 1$ for simplicity) leading to an unpolarized system with balanced spin populations, $\langle n_{i,\uparrow} \rangle = \langle n_{i,\downarrow} \rangle = n/2$, we give a schematic diagram on 2D square lattice (see Fig. 1(a)). We defined the anisotropy parameter $\alpha \in [0, 1]$, so that $\alpha = 1$ corresponds to the isotropic Hubbard model with C_4 symmetry and $\alpha = 0$ is the extreme anisotropy limit with C_2 symmetry where fermions can only move in one direction. In Methods, we establish the definitions for all the correlation functions used in our study. When fermions are fully paired in the $|U| \gg t$ limit can mapping to an effective boson $J - K$ model [16, 17]. Model mapping and correlation function of CPQMC are discussed in the Supplemental Material (SM) [21].

At zero temperature, we observe a diverse phase diagram, as depicted in Fig. 1(b). The exotic CPBM phase persists from small filling to close to half filling in regions of strong anisotropy, where a spin-dependent anisotropy suppresses the conventional s -wave pairing. It can coexisting with incommensurate density wave (IDW) phase

in extremely strong anisotropy. In regimes characterized by low and medium anisotropy, s-SF dominates. Fig. 1(c)-(d) illustrate the characteristics of the CPBM in different filling, and Fig. 1(e)-(f) represents s-SF, and IDW phases in momentum space under different parameter conditions. The presence of a nonzero momentum continuous Bose surface serves as clear evidence for the CPBM phase, as depicted in Fig. 1(c) and (d), where uncondensed Cooper pairs are evident in the s -wave pair momentum distribution function $N_{s\text{-pair}}(\mathbf{k})$. The s-SF phase exhibits a condensed peak at zero momentum in $N_{s\text{-pair}}(\mathbf{k})$, as shown in Fig. 1(e). Fig. 1(f) demonstrates the IDW phase's peak at the nonzero momentum point

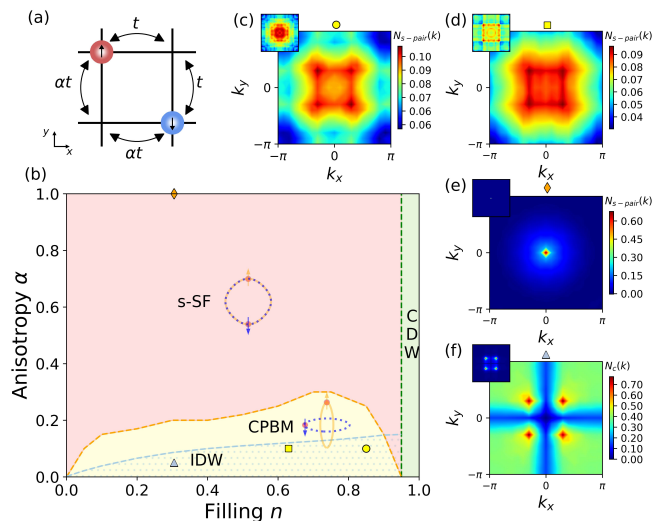


FIG. 1. (Color online) Model and phase diagram. (a). Illustration of the model with spin-dependent anisotropic hopping amplitudes on a square lattice. (b). Schematic zero-temperature phase diagram at $U = -3$ (the unit is t), exotic Cooper pair Bose metal (CPBM) exists in strong anisotropy, and IDW is an incommensurate density wave at slightly strong anisotropy range evolving to a charge density wave (CDW) close to half filling. The transition from conventional s -wave superfluid (s-SF) to CPBM is induced by increasing anisotropy. The inset show the illustration of s -wave pairing by up and down spins, and nonzero momentum s -wave pairing by up and down spins. Four different styles of markers mark the parameters we plot in (c-f) for representative case in different phases. Colored regions delimited by dotted lines indicate the qualitative boundary of different phases, which we do not claim the preciseness. (c). CPQMC simulation result of the s -wave pair momentum distribution function $N_{s\text{-pair}}(\mathbf{k})$ for $\alpha = 0.10$ at $n = 0.85$ on 20×20 lattice, showing obviously existence of nonzero momentum Bose surface, which is the signal for determining the exotic CPBM phase. The inset shows the FRG result in the thermodynamic limit, finding evidence for the existence of a nonzero momentum Bose surface using the same parameter. (d). CPBM phase for $\alpha = 0.10$ at $n = 0.63$. (e). s-SF phase on $\alpha = 1.00$ at $n = 0.305$. (f). IDW phase for $\alpha = 0.05$ at $n = 0.305$. The determination of each phase region in the phase diagram is inferred from our CPQMC data.

$\mathbf{Q} = (2k_F, 2k_F)$ of the charge structure factor $N_c(\mathbf{k})$. Further details on determining the various phase regions in the phase diagram from CPQMC data are presented in the SM [21].

CPBM is an exotic non-superfluid paired state of fermions, exhibiting some metallic properties, the Cooper pairs would form a collective state with low-energy gapless excitations along a Bose surface, with the uncondensed bosons [16, 17]. We have found evidence of Bose surface exist in the regime of intermediate U and strong hopping anisotropy at wide range of filling. We find that the CPBM phase only exists near $U \sim -3$, a small attraction is insufficient to form pairing is a metallic state, while a large attraction results in a conventional superfluid phase. Furthermore, the presence of open anisotropic Fermi surfaces promotes the formation of the Bose surface, which requires a significant anisotropy of the Fermi surface and a substantial filling.

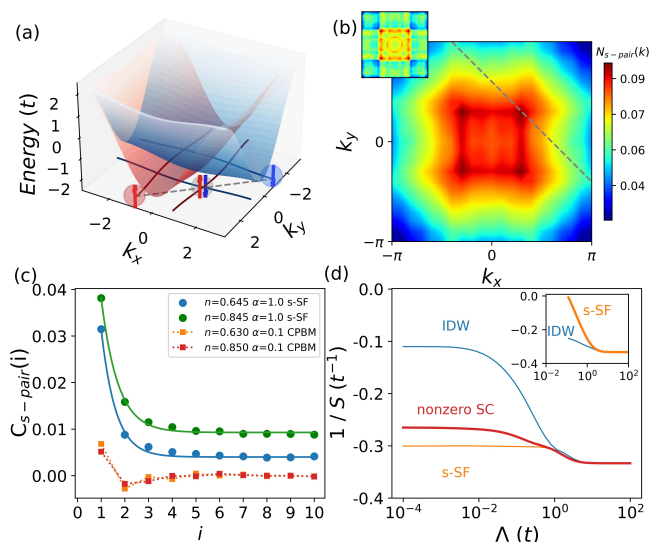


FIG. 2. (Color online) Characteristic of CPBM phase. (a). Non-interacting energy spectrum of the spin-dependent Fermi surface with anisotropy $\alpha = 0.10$ and filling $n = 0.63$. The Fermi surface is projected as red (blue) lines for the up-spin (down-spin). We provide an illustration of pairing with nonzero momentum. (b). CPQMC simulation and FRG results of pair momentum distribution function $N_{s\text{-pair}}(\mathbf{k})$ for $\alpha = 0.10$ at $n = 0.63$ with $U = -3$ on 20×20 lattice, showing existence of nonzero momentum Bose surface, which is the signal for determining the exotic CPBM phase. The gray dashed line corresponds to that in **a**. (c). The s-wave pairing correlation function in the CPBM phase and the s-SF phase in real space. The solid blue line is an exponential fitting curve. (d). The negative leading eigenvalues (NLE) S ($S < 0$) with the flow of energy cut off Λ in the CPBM phase with $\alpha = 0.10$ at $n = 0.63$. S in all phases are not divergent. The thick red line denotes the nonzero s-wave pairing mode, which is the largest pairing modes except for IDW. The inset shows the flow of S in s-SF phase with $\alpha = 1.0$ at $n = 0.63$, the thick orange line denotes the eventually diverging s-wave pairing mode.

We demonstrate the non-interacting energy dispersion for $\alpha = 0.10$ in Fig. 2(a). The solid red and blue lines below indicate the open anisotropic Fermi surface for a projection at $n = 0.63$. Due to the severe mismatch on the Fermi surface, fermions close to Fermi surface unfavors forming pairs at zero momentum. Conversely, there are pairing tendencies at finite momentum, $\mathbf{k}_{pair} = \mathbf{k}_F^\uparrow - \mathbf{k}_F^\downarrow$. We provide an illustration of nonzero momentum pairing in Fig. 2(a). Pairs with different finite momentum are formed by the fermion at different parts of anisotropic Fermi surfaces, constituting a stable continuous Bose surface with singular pair distribution function, as shown in Fig. 2(b), the weight of pairing is relatively evenly distributed on the Bose surface. The size and clarity of the Bose surface are regulated by the filling n and hopping anisotropy α . Particularly, in a highly anisotropic regime ($\alpha < 0.30$), Bose surfaces become notably prominent at a filling fraction of $n \sim 0.8$. We fix $n \sim 0.63$ and change α (Fig. S2 in SM), we observe that nonzero momentum peaks only appear in strong anisotropy ($\alpha < 0.25$), and as anisotropy increases, a more pronounced and larger complete Bose surface is formed. Fig. 2(c) compares the CPQMC simulation results of the pair correlation function for CPBM phase and s-SF phase in real space. The correlation in real space decay to zero quickly in CPBM regime and fluctuate around zero with increasing distance, showing that correlation is short-range. In s-SF regime, the correlation shows an exponential decay, and converges to a steady finite value at long distance, this is the hallmark of the long-range correlation among Cooper pairs.

CPBM exhibits unique features that distinguish it from conventional superfluids and other unconventional superfluid states such as the inhomogeneous Fulde-Ferrell-Larkin-Ovchinnikov (FFLO) pairing state [22, 23] and the homogeneous Sarma state [24, 25]. In conventional superfluids, the presence of condensed Cooper pairs is characterized by a singular peak of N_{pair} at zero momentum, contrasting with the finite momentum peaks observed in the CPBM phase. Unlike other superfluids with finite momentum pairing, CPBM does not require system polarization. In systems with polarization, pairing may occur either between fermions near mismatched Fermi surfaces to form FFLO states with Cooper pairs possessing finite momentum, or involve particles within the larger Fermi sea to establish the Sarma state with gapless fermionic excitations. More generally, the phase coherence among Cooper pairs is a key to distinguishing the CPBM phase and the FFLO state.

FRG provides additional evidence of the CPBM phase, showing signals of peaked eigenvalues at nonzero momenta in the s-wave pairing channel, as shown in inset Fig. 2(b). Fig. 2(d) shows the flow of negative leading eigenvalues (NLE) S ($S < 0$) in the CPBM phase. The decrease of the S with the flow of the energy cut off Λ , indicates the enhancement of fluctuation in the corresponding channel, and the divergence of which signals an emerging order at the associated scattering momentum.

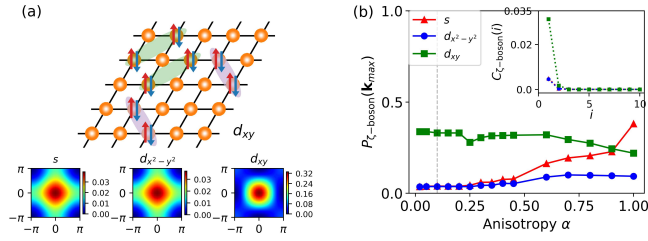


FIG. 3. (Color online) d -wave boson correlation. (a). (up panel) A schematic of the two-boson (on site pairing) d_{xy} -wave pairing in square lattice. (down panel) Two-boson correlator $P_{s-boson}(\mathbf{k})$, $P_{d_{x^2-y^2}-boson}(\mathbf{k})$, $P_{d_{xy}-boson}(\mathbf{k})$ for $\alpha = 0.10$ at $n = 0.63$ with $U = -3$ on 20×20 lattice. (b). The strength of three pairing modes of bosons paired correlation at $n \sim 0.63$ varies by anisotropy α . The inset shows boson pairing correlations in the real space (consistent with a down panel), which marked by black dashed lines.

The thick red line denotes the nonzero s -wave pairing mode, which is the largest pairing modes except for the light blue line which denotes the IDW in particle-hole (PH) channel, indicating the nonzero momentum SC is the highest pairing mode in particle-particle (PP) channel. In comparison, the inset shows the flow of s -SF phase with $\alpha = 1.0$ at $n = 0.63$, the thick orange line denotes the eventually diverging s -wave pairing mode.

Another prospect of the Bose metal phase is its d -wave correlation between bosons (on-site pairing) [17]. The d -wave here specifically refers to d_{xy} -orbital symmetry, which exhibits a propensity to introduce d -wave correlations into the system and qualitatively alter the sign structure of the electronic ground state. We defined the two-boson correlator $P_{\zeta-boson}(\mathbf{k})$ to study the possibility of a phase of paired Cooper pairs. We explored the existence of boson correlation, and bosons can be paired with both s -wave symmetry and d -wave symmetry, including $d_{x^2-y^2}$ and d_{xy} -wave. In Fig. 3(a) (up panel), we give a schematic of the two-boson d_{xy} -wave pairing correlations on the diagonals in square lattice. We show the CPQMC simulation results of two-boson correlator $P_{\zeta-boson}(\mathbf{k})$ in momentum space for $\alpha = 0.10$ at $n = 0.63$ (Consistent with the parameters of CPBM in Fig. 2(b)), $\zeta = s, d_{x^2-y^2}, d_{xy}$ (Fig. 3(a) down panel), respectively.

We demonstrated changes in the strength of three pairing modes of boson paired correlation by different anisotropy (Fig. 3(b)). The primary competition arises between s -wave and d_{xy} -wave, while $d_{x^2-y^2}$ -wave holds relatively less significance with a small value. As the anisotropy α increases, the system tends toward d_{xy} correlation between Cooper pairs. This exotic phase of boson-paired states can be termed the d -wave boson-paired state or d -wave boson liquid [17, 26]. In the inset of Fig. 3(b), we compare the correlations between boson pairs in real space. They all decay rapidly to zero in the CPBM regime, indicating short-range correlation. d_{xy} -wave exhibits the highest magnitude, suggesting its predominant boson pairing mode. Our results suggest that

the correlation between Cooper pairs is predominantly d_{xy} -wave in the CPBM regime with large anisotropy.

The extreme anisotropy leads to the exotic CPBM phase, while large anisotropy also induces the incommensurate density wave. The rich phase diagram results from the interplay between fermionic filling and Fermi surface anisotropy. In this context, the $J-K$ model corresponds to only some aspects of our system. Specific density $n = 1.2$ has been studied using the diagrammatic Monte Carlo [27] method to explore a phase diagram except s -SF and IDW phase, and two different p -wave triplet superfluid states with different symmetries have found. Additionally, the 2D attractive Hubbard model is known to be dominated by s -wave superfluidity in the absence of anisotropy [28]. In our study, we did not find any regions dominated by p -wave in the moderately anisotropic region. As the strength of anisotropy increases, the s -SF naturally transforms into the CPBM phase in particle-particle channel.

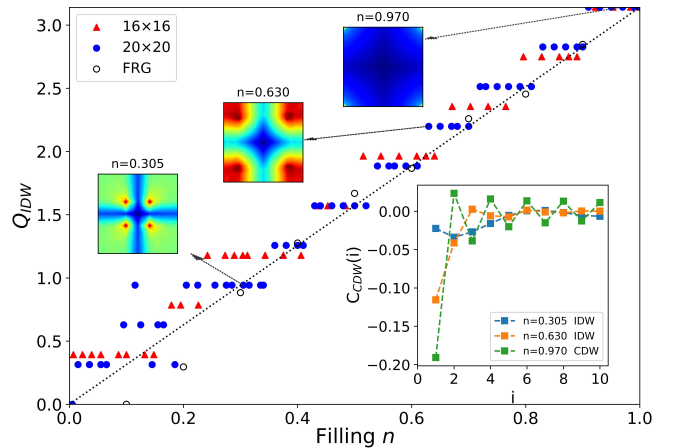


FIG. 4. (Color online) Charge density wave and incommensurate density wave. The charge structure factor for $\alpha = 0.05$ with different n at $U = -3$. As n increasing, IDW condenses at non zero momentum point $\mathbf{Q} = (2k_F, 2k_F)$, gradually diffusing to point $\mathbf{Q} = (\pi, \pi)$ convert to CDW, Q_{IDW} is the condensation point in the Brillouin zone. The upper insets show the charge structure factor of the representative IDW to CDW at $n = 0.305, 0.630, 0.970$ on 20×20 lattice, respectively. The bottom inset gives the correlation of charge density wave C_{CDW} in real space, representing IDW and CDW phase and there is no significant difference from IDW to CDW. In particular, CDW have $2a$ (lattice constant) periodic modulation of electron density in real space.

Furthermore, we find a very strong commensurate CDW state in particle-hole channel condensed at $\mathbf{Q} = (\pi, \pi)$, which is coexisting with s -SF partly. While away from half filling, IDW along the lattice diagonals exists at strong anisotropy, and having singular features condenses at nonzero momentum point $\mathbf{Q} = (2k_F, 2k_F)$. Fermi momentum k_F , which is defined as the highest momentum with occupied fermions, the density correlation is expected to oscillate with $2k_F$ wave vector. Fig. 4 shows

IDW condensed at nonzero momentum point $\mathbf{Q} = (2k_F, 2k_F)$, gradually diffusing to point $\mathbf{Q} = (\pi, \pi)$ convert to CDW as n increases, CPQMC simulation and FRG results all unanimously support this inference (more details are provided in the SM [21]). The upper insets of Fig. 4 show the charge structure factor of the representative IDW to CDW at $n = 0.305, 0.630, 0.970$ respectively. We show IDW and CDW have algebraically decaying density correlation in real space in bottom inset of Fig. 4, and it is long-range order of periodic modulation of electron density. As IDW exhibits condensation at varying momenta for different fillings, we anticipate that large anisotropy would tend to form condensate at momenta $2k_F$ associated with the Fermi surface nesting, especially in the presence of small fillings.

The realization of the CPBM is feasible in optical lattice experiments through tuning the filling and hopping anisotropy of effective spin interactions with light. This has been achieved, and the experimentalists can tune the interparticle interactions to arbitrary values using a Feshbach resonance of tunable few-fermion systems [29], particularly using laser-dressed Rydberg atoms experiments with spin-dependent hyperfine states can reveal their highly tunable range and anisotropy [30, 31]. Although few-body systems with dipole-dipole interactions have not been studied experimentally as of yet, some theoretical studies of a small ensemble of dipolar bosons are already under investigation [32, 33], which can observe d -wave correlation between bosons. A recent research observes and quantifies the pseudogap in unitary Fermi gases of lithium-6 atoms through momentum-resolved microwave spectroscopy [34]. They lend support for the role of preformed pairing as a precursor to superfluidity. This again offers another ideal quantum simulators to study the proposed Bose metal phase. Moreover, in thin films of $\text{YBa}_2\text{Cu}_3\text{O}_{7-x}$, a robust anomalous metallic state was detected between the superconducting and insulating regimes, characterized by the charge- $2e$ quantum oscillation that is potentially linked to the existence of Bose liquid [35].

To summarize, we confirm the existence of the exotic

CPBM phase with d -wave correlation between Cooper pairs by an attractively interacting fermionic system with hopping anisotropy between two species of spins in 2D lattice. While away from half filling, IDW along the lattice diagonals exists at strong anisotropy, and having singular features condense at nonzero momentum point $\mathbf{Q} = (2k_F, 2k_F)$, gradually diffusing to $\mathbf{Q} = (\pi, \pi)$ become CDW as n increases to half filling. Our results strongly suggest the competition of driving force behind the formation of exotic phases, by the Fermi surface anisotropy or the filling.

In recent years, in the realm of condensed matter, the investigation of spin-dependent anisotropic Fermi surfaces has been extensive, particularly in the context of altermagnetism [36, 37]—a spin-splitting phenomenon with collinear magnetic order incompatible with conventional ferromagnetism or antiferromagnetism. Through the low-frequency phonons [38], electron-phonon coupling [39] or spin-phonon coupling [40, 41] provides a weak attractive potential, greatly affecting the properties of magnetic materials. Materials such as RuO_2 , KRu_4O_8 , and La_2CuO_4 are potential candidate exhibiting altermagnetic spin splitting, herein spin-Fermi surface anisotropy plays an important role. The spin-dependent anisotropy found in cuprate again suggests the intricate link between its unconventional superconductivity, strong correlations and Fermi surface anisotropy, warranting further investigation.

We acknowledge useful discussion with Noah F. Q. Yuan. This work is supported by National Natural Science Foundation of China (No. 12204130, No. 12088101), National Key Research and Development Program of China (No. 2022YFA1402701). H.K.T acknowledges supports from Shenzhen Start-Up Research Funds (No. HA11409065) and Shenzhen Key Laboratory of Advanced Functional Carbon Materials Research and Comprehensive Application (No. ZDSYS20220527171407017). J.-H.S. acknowledges supports from the Ningbo Natural Science Fund (No. 2023J131). T.Y. acknowledges supports from Natural Science Foundation of Heilongjiang Province (No. YQ2023A004).

-
- [1] J. G. Bednorz and K. A. Müller, Possible high T_c superconductivity in the Ba–La–Cu–O system, *Z Physik B* **64**, 189 (1986).
 - [2] L. D. Landau, The theory of a fermi liquid, *Sov. Phys. JETP* **3**, 920 (1957).
 - [3] P. A. Lee, N. Nagaosa, and X.-G. Wen, Doping a Mott insulator: Physics of high-temperature superconductivity, *Rev. Mod. Phys.* **78**, 17 (2006).
 - [4] B. Keimer, S. A. Kivelson, M. R. Norman, S. Uchida, and J. Zaanen, From quantum matter to high-temperature superconductivity in copper oxides, *Nature* **518**, 179 (2015).
 - [5] N. Singh, Leading theories of the cuprate superconductivity: A critique, *Physica C Supercond* **580**, 1353782 (2021).
 - [6] P. W. Anderson, The Resonating Valence Bond State in La_2CuO_4 and Superconductivity, *Science* **235**, 1196 (1987).
 - [7] T. Dahm, V. Hinkov, S. V. Borisenko, A. A. Kordyuk, V. B. Zabolotnyy, J. Fink, B. Büchner, D. J. Scalapino, W. Hanke, and B. Keimer, Strength of the spin-fluctuation-mediated pairing interaction in a high-temperature superconductor, *Nat. Phys.* **5**, 217 (2009).
 - [8] P. W. Phillips, N. E. Hussey, and P. Abbamonte, Stranger than metals, *Science* **377**, eabh4273 (2022).
 - [9] Y. Zhou, K. Kanoda, and T.-K. Ng, Quantum spin liquid states, *Rev. Mod. Phys.* **89**, 025003 (2017).
 - [10] C. Broholm, R. J. Cava, S. A. Kivelson, D. G. Nocera,

- M. R. Norman, and T. Senthil, Quantum spin liquids, *Science* **367**, 10.1126/science.aay0668 (2020).
- [11] P. Phillips and D. Dalidovich, The elusive Bose metal, *Science* **302**, 243 (2003).
- [12] O. I. Motrunich and M. P. A. Fisher, d -wave correlated critical Bose liquids in two dimensions, *Physical review. B, Condensed matter* **75**, 235116 (2007).
- [13] M. S. Block, R. V. Mishmash, R. K. Kaul, D. N. Sheng, O. I. Motrunich, and M. P. A. Fisher, Exotic gapless mott insulators of bosons on multileg ladders, *Physical review letters* **106**, 046402 (2011).
- [14] R. V. Mishmash, M. S. Block, R. K. Kaul, D. N. Sheng, O. I. Motrunich, and M. P. A. Fisher, Bose metals and insulators on multileg ladders with ring exchange, *Physical review. B, Condensed matter* **84**, 245127 (2011).
- [15] H.-C. Jiang, M. S. Block, R. V. Mishmash, J. R. Garrison, D. N. Sheng, O. I. Motrunich, and M. P. A. Fisher, Non-Fermi-liquid d -wave metal phase of strongly interacting electrons, *Nature* **493**, 39 (2013).
- [16] A. E. Feiguin and M. P. A. Fisher, Exotic paired states with anisotropic spin-dependent Fermi surfaces, *Phys. Rev. Lett.* **103**, 025303 (2009).
- [17] A. E. Feiguin and M. P. A. Fisher, Exotic paired phases in ladders with spin-dependent hopping, *Physical review. B, Condensed matter* **83**, 115104 (2011).
- [18] M. S. Block, D. N. Sheng, O. I. Motrunich, and M. P. A. Fisher, Spin Bose-metal and valence bond solid phases in a spin-1/2 model with ring exchanges on a four-leg triangular ladder, *Physical review letters* **106**, 157202 (2011).
- [19] S. Zhang, J. Carlson, and J. E. Gubernatis, Constrained path quantum Monte Carlo method for fermion ground states, *Physical review letters* **74**, 3652 (1995).
- [20] C. Wetterich, Average action and the renormalization group equations, *Nuclear Physics B* **352**, 529 (1991).
- [21] See Supplemental Material, which includes Refs. [42–44], for details on the method and additional simulation results.
- [22] P. Fulde and R. A. Ferrell, Superconductivity in a Strong Spin-Exchange Field, *Physics Review* **135**, A550 (1964).
- [23] A. Larkin, Superconductor of small dimensions in a strong magnetic field, *Soviet Physics JETP* **21**, 153 (1965).
- [24] G. Sarma, On the influence of a uniform exchange field acting on the spins of the conduction electrons in a superconductor, *The Journal of physics and chemistry of solids* **24**, 1029 (1963).
- [25] M. M. Forbes, E. Gubankova, W. V. Liu, and F. Wilczek, Stability criteria for breached-pair superfluidity, *Phys. Rev. Lett.* **94**, 017001 (2005).
- [26] D. N. Sheng, O. I. Motrunich, S. Trebst, E. Gull, and M. P. A. Fisher, Strong-coupling phases of frustrated bosons on a two-leg ladder with ring exchange, *Phys. Rev. B* **78**, 054520 (2008).
- [27] J. Gukelberger, E. Kozik, L. Pollet, N. Prokof'ev, M. Sigrist, B. Svistunov, and M. Troyer, p -Wave superfluidity by spin-nematic Fermi surface deformation, *Physical review letters* **113**, 195301 (2014).
- [28] T. Paiva, R. R. dos Santos, R. T. Scalettar, and P. J. H. Denteneer, Critical temperature for the two-dimensional attractive Hubbard model, *Physical review. B, Condensed matter* **69**, 184501 (2004).
- [29] F. Serwane, G. Zürn, T. Lompe, T. B. Ottenstein, A. N. Wenz, and S. Jochim, Deterministic preparation of a tunable few-fermion system, *Science* **332**, 336 (2011).
- [30] Y.-Y. Jau, A. M. Hankin, T. Keating, I. H. Deutsch, and G. W. Biedermann, Entangling atomic spins with a Rydberg-dressed spin-flip blockade, *Nature physics* **12**, 71 (2015).
- [31] J. Zeiher, R. van Bijnen, P. Schauß, S. Hild, J.-Y. Choi, T. Pohl, I. Bloch, and C. Gross, Many-body interferometry of a Rydberg-dressed spin lattice, *Nature physics* **12**, 1095 (2016).
- [32] B. Chatterjee, M. C. Tsatsos, and A. U. J. Lode, Correlations of strongly interacting one-dimensional ultracold dipolar few-boson systems in optical lattices, *New J. Phys.* **21**, 033030 (2019).
- [33] B. Chatterjee and A. U. J. Lode, Order parameter and detection for a finite ensemble of crystallized one-dimensional dipolar bosons in optical lattices, *Phys. Rev. A* **98**, 053624 (2018).
- [34] X. Li, S. Wang, X. Luo, Y.-Y. Zhou, K. Xie, H.-C. Shen, Y.-Z. Nie, Q. Chen, H. Hu, Y.-A. Chen, X.-C. Yao, and J.-W. Pan, Observation and quantification of the pseudogap in unitary Fermi gases, *Nature* **626**, 288 (2024).
- [35] C. Yang, Y. Liu, Y. Wang, L. Feng, Q. He, J. Sun, Y. Tang, C. Wu, J. Xiong, W. Zhang, X. Lin, H. Yao, H. Liu, G. Fernandes, J. Xu, J. M. Valles, Jr, J. Wang, and Y. Li, Intermediate bosonic metallic state in the superconductor-insulator transition, *Science* **366**, 1505 (2019).
- [36] L. Šmejkal, J. Sinova, and T. Jungwirth, Emerging research landscape of altermagnetism, *Phys. Rev. X* **12**, 040501 (2022).
- [37] L. Šmejkal, J. Sinova, and T. Jungwirth, Beyond conventional ferromagnetism and antiferromagnetism: A phase with nonrelativistic spin and crystal rotation symmetry, *Phys. Rev. X* **12**, 031042 (2022).
- [38] M. Uchida, T. Nomoto, M. Musashi, R. Arita, and M. Kawasaki, Superconductivity in Uniquely Strained RuO₂ Films, *Phys. Rev. Lett.* **125**, 147001 (2020).
- [39] O. Rösch, O. Gunnarsson, X. J. Zhou, T. Yoshida, T. Sasagawa, A. Fujimori, Z. Hussain, Z.-X. Shen, and S. Uchida, Polaronic behavior of undoped high- T_c cuprate superconductors from angle-resolved photoemission spectra, *Phys. Rev. Lett.* **95**, 227002 (2005).
- [40] A. al Wahish, K. R. O'Neal, C. Lee, S. Fan, K. Hughey, M. O. Yokosuk, A. J. Clune, Z. Li, J. A. Schlueter, J. L. Manson, M.-H. Whangbo, and J. L. Musfeldt, Magnetic phase transitions and magnetoelastic coupling in $s = \frac{1}{2}$ heisenberg antiferromagnets, *Phys. Rev. B* **95**, 104437 (2017).
- [41] J. Choe, D. Lujan, M. Rodriguez-Vega, Z. Ye, A. Leonardo, J. Quan, T. N. Nunley, L.-J. Chang, S.-F. Lee, J. Yan, G. A. Fiete, R. He, and X. Li, Electron-Phonon and Spin-Lattice Coupling in Atomically Thin Layers of MnBi₂Te₄, *Nano Lett.* **21**, 6139 (2021).
- [42] S. Zhang, J. Carlson, and J. E. Gubernatis, Constrained path Monte Carlo method for fermion ground states, *Physical review. B, Condensed matter* **55**, 7464 (1997).
- [43] W.-S. Wang, Y.-Y. Xiang, Q.-H. Wang, F. Wang, F. Yang, and D.-H. Lee, Functional renormalization group and variational Monte Carlo studies of the electronic instabilities in graphene near 1/4 doping, *Phys. Rev. B* **85**, 035414 (2012).
- [44] W.-S. Wang, C.-C. Zhang, F.-C. Zhang, and Q.-H. Wang, Theory of Chiral p -Wave Superconductivity with Near Nodes for Sr₂RuO₄, *Phys. Rev. Lett.* **122**, 027002 (2019).

Supplemental Material for "Exotic d-wave Bose Metal in two dimensions"

Zhangkai Cao,^{1,*} Jiahao Su,^{1,2,*} Jianyu Li,^{1,2} Tao Ying,³ WanSheng Wang,^{4,†} Jin-Hua Sun^{*,4,‡} Ho-Kin Tang,^{1,2,§} and Haiqing Lin⁵

¹*School of Science, Harbin Institute of Technology, Shenzhen, 518055, China*

²*Shenzhen Key Laboratory of Advanced Functional Carbon Materials Research and Comprehensive Application, Shenzhen 518055, China.*

³*School of Physics, Harbin Institute of Technology, Harbin 150001, China*

⁴*Department of Physics, Ningbo University, Ningbo 315211, China*

⁵*Institute for Advanced Study in Physics and School of Physics, Zhejiang University, Hangzhou, 310058, China.*

(Dated: May 27, 2024)

In this Supplemental Material, we present additional computational results. In Sec. S1, we introduce the connection between our model of spin-dependent fermions to the $J - K$ model and $t - J - K$ model. In Sec. S2, we have defined various correlation functions. In Sec. S3, we mainly introduces how to determine various phase regions in the phase diagram from the CPQMC data. We discuss how to determine the CPBM phase from the CPQMC data and show comparison of charge density momentum distribution function of CPQMC and FRG to support the presence of IDW and CDW. In Sec. S4, we discuss the boson correlation of various phases. In Sec. S5, we gave a brief introduction to Constraint path quantum Monte Carlo. In addition, we discuss the implementation of CPQMC, including the formalism, hyper-parameters and parallelization that is quite necessary for large lattice simulation. In Sec. S6, we also gave a brief introduction to Functional renormalization group method, which provided us with reliable supporting evidence to determine the CPBM phase.

S1. Model mapping

The connection between our model of spin-dependent fermions to the $J - K$ model is made as the following. When $|U| \gg t$, where consider all of the fermions are tightly bound into on-site Cooper pairs. We can derive an effective boson Hamiltonian by considering a perturbation expansion in powers of $t/|U|$ [S1–S3]. In subspaces containing only empty occupancy and paired double occupancy, the effective Hamiltonian can be written as: $H_b = -J \sum_{i,j} b_i^\dagger b_j + K \sum_{ring} b_1^\dagger b_2 b_3^\dagger b_4 + h.c.$. Here, $b_i^\dagger = c_{i\uparrow}^\dagger c_{i\downarrow}^\dagger$, and $i = 1, 2, 3, 4$ labeling sites taken clockwise around a square plaquette. In addition to the usual second-order near neighbor boson hopping term with strength $J = 2\alpha t^2/|U|$, one obtains a more important fourth-order four-site "ring" exchange term with strength $K = (t^4 + 2\alpha^2 t^4 + \alpha^4 t^4)/|U|^3$, so called $J - K$ model [S2, S3]. Remarkably, while the hopping term in the extreme anisotropic limit, $\alpha \rightarrow 0$, so $J \rightarrow 0$, but the ring exchange term K which hops pairs of bosons is nonzero. Thus, with increasing anisotropy, we can obtain the ratio $K/J = \frac{1+2\alpha^2+\alpha^4}{\alpha} t^2/|U|^2$ increases, and the ring exchange term becomes increasingly important in the total Hamiltonian H_b . In other words, the magnitude of K is regulated by anisotropy α in our model.

In $t - J - K$ model [S4], we first write the electron operator for a bosonic chargon $b(\mathbf{r})$ and fermionic spinon $f_s(\mathbf{r})$, so exactly a chargon and one spinon to compose an electron. Then, we decompose the hard-core boson as $b(\mathbf{r}) = d_1(\mathbf{r})d_2(\mathbf{r})$, where d_1 and d_2 are fermionic slave particles (partons) with anisotropic hopping patterns, $d_1(d_2)$ is chosen to hop preferentially in the $x(y)$ direction. The electron can written an all-fermionic decomposition format: $c(\mathbf{r}) = d_1(\mathbf{r})d_2(\mathbf{r})f_s(\mathbf{r})$. The resulting theory now includes two gauge fields: one to glue together d_1 and d_2 to form the chargon and another to glue together b and f to form the electron, the first gauge field combine two anisotropic partons to a bosonic chargon, which is the focus of our attention. The assumption of a positive value for K is crucial in the model to realize the d-wave metal. More ab-initio calculations on realistic cuprate could give a reliable estimate of the sign of K as well as its magnitude. Within a gauge theory framework in $J - K$ model, the picture of the Bose metal phase consists of two independent species of fermions hopping on the square lattice with anisotropic hopping, the attractive potential U provides an attractive pairing for bosons. The four-site ring exchange term $K = (t^4 + 2\alpha^2 t^4 + \alpha^4 t^4)/|U|^3 > 0$ in $J - K$ model are four-spin (eight-fermion) terms and can arise from the attractive U . In contrast to $t - J - K$ model, the electron ring term K are four-fermion terms, which move two charges from one diagonal of a square to the other previously unoccupied diagonal. Thus the electron ring term K can arise from the long-range Coulomb interaction. The strength of the electron ring term increases with increasing

* These authors contributed equally

† wangwansheng@nbu.edu.cn

‡ sunjinhua@nbu.edu.cn

§ denghaojian@hit.edu.cn

hopping anisotropy between the d_1 and d_2 partons. The attraction here originates from the gauge interaction between the fermionic partons, resulting in bosonic chargon in the slave-particle gauge theory.

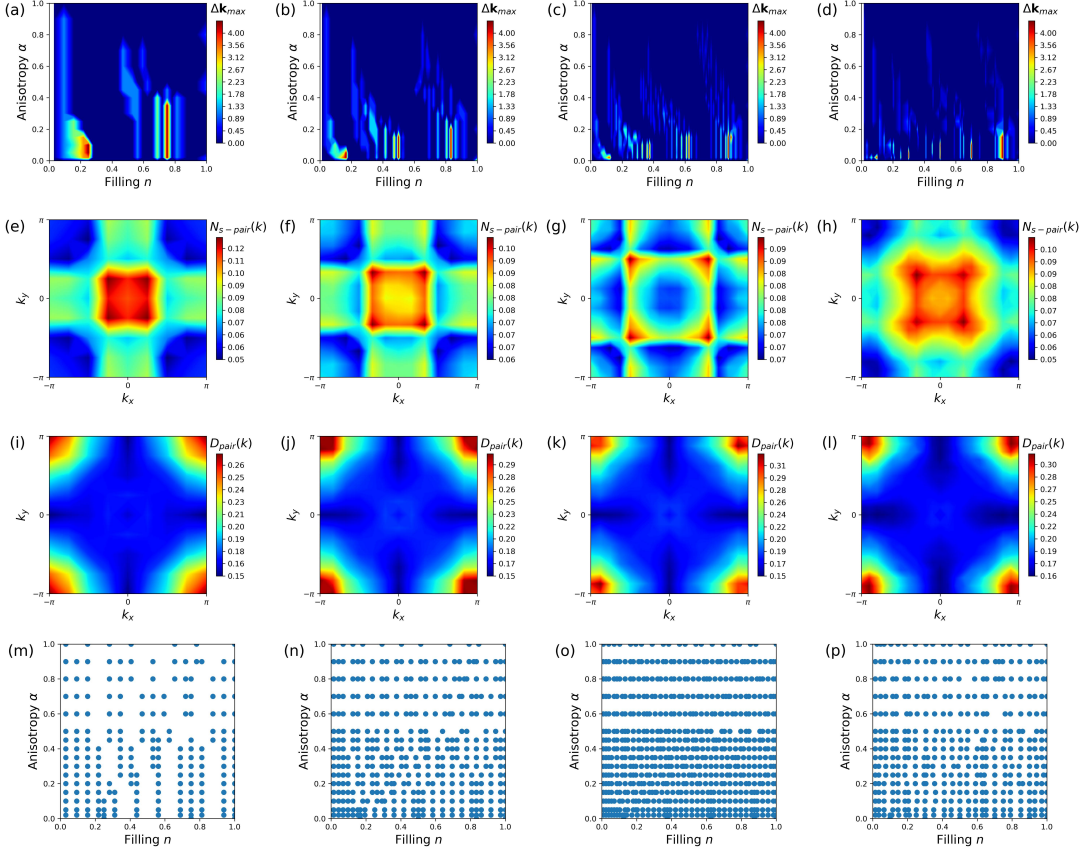


FIG. S1. (Color online) Determination of the CPBM. (a-d). CPQMC simulation result for determine the region of CPBM at $U = -3$ on 8×8 , 12×12 , 16×16 , 20×20 lattice, where $\Delta \mathbf{k}_{\max} = \sqrt{\mathbf{k}_{\max}^2(x) + \mathbf{k}_{\max}^2(y)}$, $\mathbf{k}_{\max}(x)$, $\mathbf{k}_{\max}(y)$ are the coordinates of the maximum value in the pair momentum distribution function. The blue areas are $\Delta \mathbf{k}_{\max} = 0$, representing the s -wave pair momentum distribution function condensed at $\mathbf{Q} = (0, 0)$, other regions are $\Delta \mathbf{k}_{\max} \neq 0$. If $\Delta \mathbf{k}_{\max} \neq 0$, it indicates that there is a nonzero momentum peak in the pair momentum distribution function, and then combined with image display to form a Bose surface, so we believe that there exist a CPBM phase under this parameter. (e-h). CPQMC simulation result of s -wave pair momentum distribution function $N_{s\text{-pair}}(\mathbf{k})$ for $\alpha = 0.10$ at $n \sim 0.85$ in $U = -3$ on 8×8 , 12×12 , 16×16 , 20×20 lattice, showing obviously existence of nonzero momentum Bose surface, which is the signal for determine the exotic CPBM phase. (i-l). CPQMC simulation results of pair density structure factor $D_{\text{pair}}(\mathbf{k})$ in same parameter conditions. Specifically, it shows a rather large peak near $\mathbf{Q} = (\pi, \pi)$, which shows the off-center peak indicate the pairing of fermions with different spins. (m-p). We marked the parameter selection of n and α on 8×8 , 12×12 , 16×16 , 20×20 lattice.

S2. Correlation function

We have defined the s -wave pair momentum distribution function

$$N_{s\text{-pair}}(\mathbf{k}) = (1/N) \sum_{i,j} \exp[i\mathbf{k}(\mathbf{r}_i - \mathbf{r}_j)] \langle \Delta_s^\dagger(i) \Delta_s(j) \rangle, \quad (\text{S1})$$

where $\Delta_s^\dagger(i) = c_{i\uparrow}^\dagger c_{i\downarrow}^\dagger$. Here N is the number of sites.

We have defined the density structure factor,

$$D_{\text{pair}}(\mathbf{k}) = (1/N) \sum_{i,j} \exp[i\mathbf{k}(\mathbf{r}_i - \mathbf{r}_j)] \langle n_{bi} n_{bj} \rangle, \quad (\text{S2})$$

Here, the Cooper pair number operator is defined as $n_{bi} = b_i^\dagger b_i = n_{i\uparrow} n_{i\downarrow}$, where $b_i^\dagger = c_{i\uparrow}^\dagger c_{i\downarrow}^\dagger$ and $n_{i\uparrow} = c_{i\uparrow}^\dagger c_{i\uparrow}$.

To study the density correlations, we defined the charge structure factor in particle-hole channel,

$$N_c(\mathbf{k}) = (1/N) \sum_{i,j} \exp[i\mathbf{k}(\mathbf{r}_i - \mathbf{r}_j)] \langle n_i n_j \rangle, \quad (\text{S3})$$

Here, the density number operator is defined as $n_i = \sum_{\sigma} c_{i\sigma}^{\dagger} c_{i\sigma}$.

The correlation function of different pairing mode in real space are defined as $C_{s-pair} = \langle \Delta_s^{\dagger}(i) \Delta_s(j) \rangle$. The correlation function of charge density wave in real space are defined as $C_{CDW} = \langle n_i n_j \rangle$.

We also defined the two-boson (on site pairing) correlator,

$$P_{\zeta-boson}(\mathbf{k}) = (1/N) \sum_{i,j} \exp[i\mathbf{k}(\mathbf{r}_i - \mathbf{r}_j)] \langle b^{\dagger}(i) b^{\dagger}(i') b(j) b(j') \rangle, \quad (\text{S4})$$

where $\zeta = s, d_{x^2-y^2}, d_{xy}$. When $\zeta = s$, $d_{x^2-y^2}$, i' or j' site is the NN sites of i or j site, and when $\zeta = d_{xy}$, i' or j' site is the next NN sites of i or j site. Among them, we focus more attention d_{xy} -wave boson correlation. The boson pairing correlations in real space are defined as $C_{\zeta-boson} = \langle b^{\dagger}(i) b^{\dagger}(i') b(j) b(j') \rangle$, where $\zeta = s, d_{x^2-y^2}, d_{xy}$.

S3. Phase diagram

This section mainly introduces how to determine various phase regions in the phase diagram from the CPQMC data.

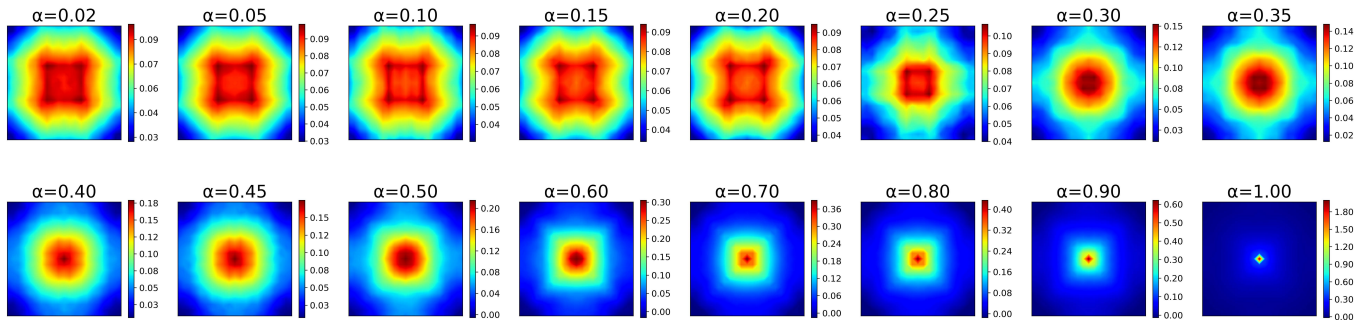


FIG. S2. (Color online) Transition of s-SF to CPBM by anisotropy. CPQMC simulation result of s -wave pair momentum distribution function $N_{s-pair}(\mathbf{k})$ from extremely anisotropy $\alpha \rightarrow 0$ to isotropic $\alpha = 1$ at $n \sim 0.63$ with $U = -3$ on 20×20 lattice. We see that nonzero momentum peaks only appear in strong anisotropy ($\alpha < 0.25$), and as anisotropy increases ($\alpha \downarrow$), a more pronounced and larger complete Bose surface is formed. When the anisotropy is weak ($\alpha > 0.90$), the system exhibits very good s-SF condensed at $\mathbf{Q} = (0, 0)$. In the middle anisotropic region ($\alpha = 0.3 - 0.8$), there are also weakened s-SF. On the whole, as the anisotropy increases, the difference of the Fermi surface by the two spin electrons also increases, leading to a tendency towards pairing at larger \mathbf{k} in the Brillouin zone, thus forming the exotic CPBM.

We have shown the determination of the CPBM region in Fig. S1(a)-(d), on 8×8 , 12×12 , 16×16 , 20×20 lattice, with non-zero peak in N_{s-pair} . We can see at small lattice size, the distribution of CPBM regimes is relatively scattered, but as the lattice size increases, the distribution area gradually expands. Because of constraints in computational resources availability, our calculations were limited to a maximum lattice size of 20×20 . From the trend of change, we expect that under infinite lattice points $N \rightarrow \infty$, the CPBM regimes will be connected as a whole, reaching its maximum critical α at $n \sim 0.8$, as shown in Fig. 1(b) in the main text. Meanwhile, we draw the Bose surface of features in CPBM phase at different lattice size in Fig. S1(e)-(h), selecting on different lattice at $U = -3$ for $\alpha = 0.10$ with $n \sim 0.85$. As the lattice size increases, the nonzero momentum Bose surface persists and its shape becomes conspicuous. We also give the pair density structure factor $D_{pair}(\mathbf{k})$ consistent with Fig. S1(e)-(h) in Fig. S1(i)-(l), which can help us understand the formation of CPBM phase. Specifically, it shows a rather large peak near $\mathbf{Q} = (\pi, \pi)$, which shows the off-center peak indicate the pairing of fermions with different spins. Fig. S2 show the transition of s-SF phase to CPBM phase caused by anisotropy α . Fig. S3 show the lattice size effect in different anisotropy α , which reflects that CPBM is a stable phase. All of these provided evidence for the existence of CPBM phase and its parameter regions.

IDW along the lattice diagonals exists at strong anisotropy, and having singular features condenses at non zero momentum point $\mathbf{Q} = (2k_F, 2k_F)$, gradually diffusing to point $\mathbf{Q} = (\pi, \pi)$ convert to CDW as n approached to

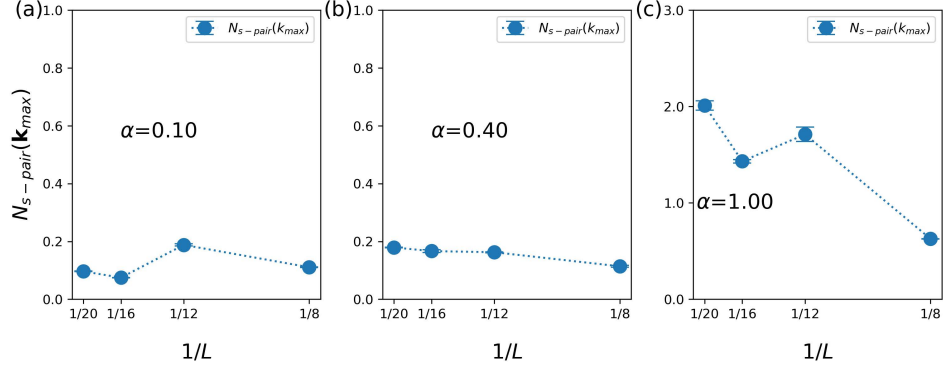


FIG. S3. (Color online) Lattice size effect in different phase. (a). CPBM for $\alpha = 0.10$, (b). s-SF for $\alpha = 0.40$, (c). s-SF for $\alpha = 1.00$ at $n \sim 0.63$ with $U = -3$ on 8×8 , 12×12 , 16×16 , 20×20 lattice. We can see that in CPBM region, the value of $N_{s-pair}(\mathbf{k}_{max})$ has always been stable, which is represent that the CPBM phase will always exist in large or even infinite lattice size. As α increases, we can clearly see that the value of $N_{s-pair}(\mathbf{k}_{max})$ increase, so s-SF is slightly suppressed at moderately anisotropic region. When $\alpha = 1.00$, we can clearly see that as the lattice size increases, the value of $N_{s-pair}(\mathbf{k}_{max})$ is continuously increasing, so s-SF is significantly diverge at weak anisotropic region.

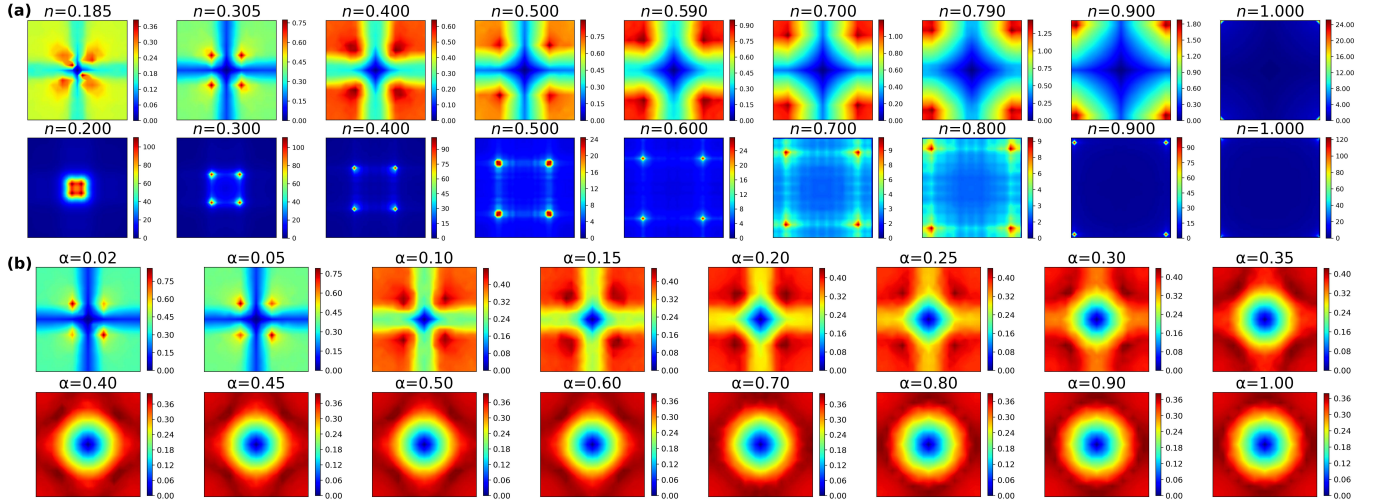


FIG. S4. (Color online) Incommensurate density wave and charge density wave. (a). CPQMC simulation result of charge structure factor by the representative IDW to CDW for $\alpha = 0.05$ at $U = -3$ with different fillings on 20×20 lattice (top panel), and the FRG result with different fillings in the thermodynamic limit (bottom panel). As n increasing, IDW along the lattice diagonals exists at strong anisotropy, and having singular features condenses at non-zero momentum point $\mathbf{Q} = (2k_F, 2k_F)$, gradually diffusing to point $\mathbf{Q} = (\pi, \pi)$ convert to CDW order as n approached to half filling, CPQMC simulation and FRG results all unanimously support this inference. (b). CPQMC simulation result of charge structure factor $N_c(\mathbf{k})$ for different α at $n \sim 0.305$ with $U = -3$ on 20×20 lattice. When $\alpha < 0.30$, it clearly condensed at $\mathbf{Q} = (2k_F, 2k_F)$, which is IDW. However, when $\alpha > 0.30$, the density wave weight disperses around the periphery of the Brillouin zone. Considering the competition between density waves with different momentum, we expect that weak anisotropy will not be conducive to the formation of momentum related to $\mathbf{Q} = (2k_F, 2k_F)$, IDW only exists in strong anisotropy. While CDW order condensed at $\mathbf{Q} = (\pi, \pi)$ close to half filling are less sensitive to change anisotropy.

half filling, CPQMC simulation and FRG results all unanimously support this inference (Fig. S4(a)). We have also provided the charge structure factor $N_c(\mathbf{k})$ for different α at $n \sim 0.305$ (with more obvious evolution) in Fig. S4(b). The boundary points of the IDW region in phase diagram are determined by whether the density waves condensed at $\mathbf{Q} = (2k_F, 2k_F)$ point with a sharp peak in momentum space, which we have clearly displayed in Fig. S5. From the finite size data in Fig. S5(a)-(d), we find the increase of condensation with lattice size in IDW phase. With larger n , IDW persists to larger anisotropy up to $\alpha = 0.10$. As n gradually increases to half filling ($n > 0.95$), we combine Fig. S5(e)-(h) and Fig. S5(i)-(l) to determine a strong CDW order exhibit, which are less sensitive to change of anisotropy. If the density wave condensed at $\mathbf{Q} = (\pi, \pi)$, IDW naturally converts to CDW in our phase diagram.

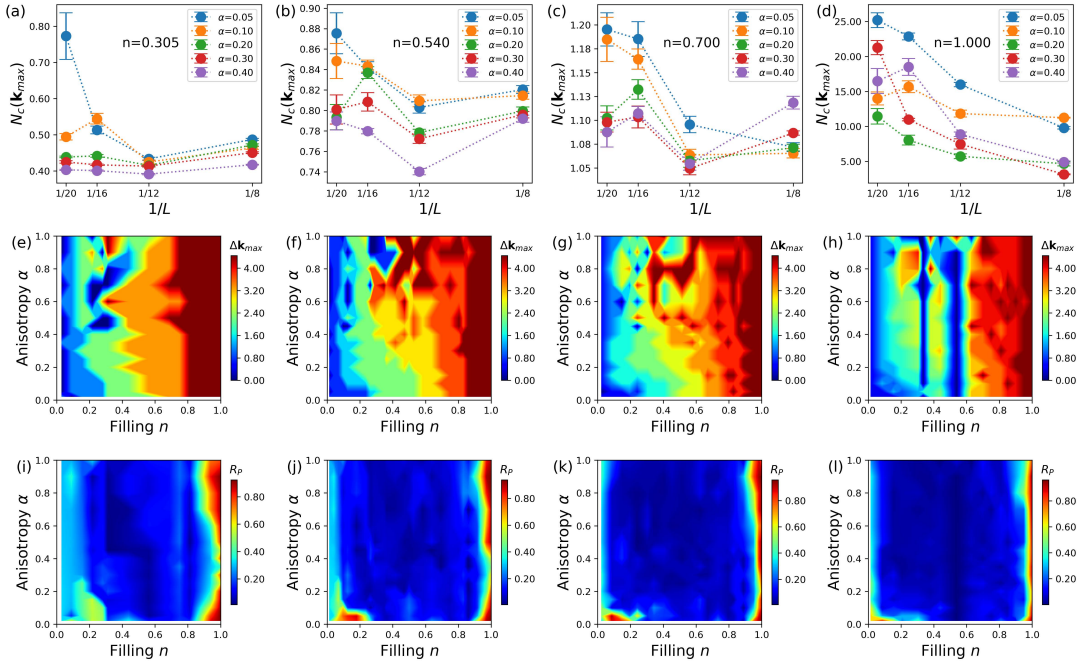


FIG. S5. (Color online) Determination of the IDW and CDW. (a-d). Lattice size effect of charge structure factor $N_c(\mathbf{k})$ for $\alpha = 0.05, 0.10, 0.20, 0.30, 0.40$ at $U = -3$ on $8 \times 8, 12 \times 12, 16 \times 16, 20 \times 20$ lattice for different n . **a**, $n \sim 0.305$, **b**, $n \sim 0.54$, **c**, $n \sim 0.70$, **d**, $n \sim 1.00$. The divergence of lattice effect represents the existence of IDW/CDW phase. (e-h). CPQMC simulation result for distinguishing IDW and CDW regions at $U = -3$ on $8 \times 8, 12 \times 12, 16 \times 16, 20 \times 20$ lattice, where $\Delta \mathbf{k}_{\max} = \sqrt{\mathbf{k}_{\max}^2(x) + \mathbf{k}_{\max}^2(y)}$, $\mathbf{k}_{\max}(x)$, $\mathbf{k}_{\max}(y)$ are the coordinates of the maximum value in the charge structure factor. When $\Delta \mathbf{k}_{\max}$ is the maximum value ($\mathbf{k}_{\max}(x) = \mathbf{k}_{\max}(y) = \pi$), the charge structure factor condensed at $\mathbf{Q} = (\pi, \pi)$ in momentum space, the system display CDW order in phase diagram. (i-l). CPQMC simulation result for determine the region of IDW and CDW at $U = -3$ on $8 \times 8, 12 \times 12, 16 \times 16, 20 \times 20$ lattice, where $R_p = \frac{p - \bar{p}}{\bar{p}}$, p is the maximum peak value in the charge structure factor and \bar{p} is the average value of the points next to the maximum peak. The blue areas are $R_p \simeq 0$, representing the charge structure factor dispersed in momentum space, not forming a peak. If $R_p \gg 0$, it indicates that the IDW condensed at $\mathbf{Q} = (2k_F, 2k_F)$ with a sharp peak, so we believe that there exist a IDW phase under this parameter. At small n ($0.05 < n < 0.2$), a relatively large peak structure appears, but the area becomes smaller as the lattice size increases, which is not a stable state due to the influence of lattice effects. When $n > 0.95$, while CDW order condensed at $\mathbf{Q} = (\pi, \pi)$ displaying a very large peak, the peak intensity may slightly decrease in the regime of intermediate anisotropy α .

S4. Boson correlation

Regardless of whether the system is in the s-SF or CPBM phase, the electrons near the Fermi surface are pairing on-site in the system. Therefore, it is important to explore the correlation between bosons (on-site pairing), especially when the system does not exhibit superfluid condensation in CPBM phase. We defined the two-boson correlator $P_{\zeta-boson}(\mathbf{k})$ to study the possibility of a phase of paired Cooper pairs. We explored the existence of boson correlation, and bosons can be paired with both s -wave symmetry, $d_{x^2-y^2}$ and d_{xy} -wave symmetry. In Fig. S6(a)-(c), we give the CPQMC simulation results of two-boson correlator $P_{\zeta-boson}(\mathbf{k})$ in momentum space for different anisotropy α at $n \sim 0.63$, $\zeta = s, d_{x^2-y^2}, d_{xy}$, respectively.

We extracted the maximum values of three pairing modes of boson paired correlation and shown in the main text Fig. 3(b) the variation of boson correlation with the strength of anisotropy. In Fig. S7, we compare the correlations between boson pairs in real space at different anisotropy. They all decay rapidly to zero, indicating that boson correlation are short-range correlation. The primary competition arises between s -wave and d_{xy} -wave, while $d_{x^2-y^2}$ -wave holds relatively less significance with a small value. Our results suggest that the correlation between Cooper pairs is predominantly d_{xy} -wave in the CPBM regime with large anisotropy. This exotic phase of boson-paired states can be termed the d-wave Bose Metal state.

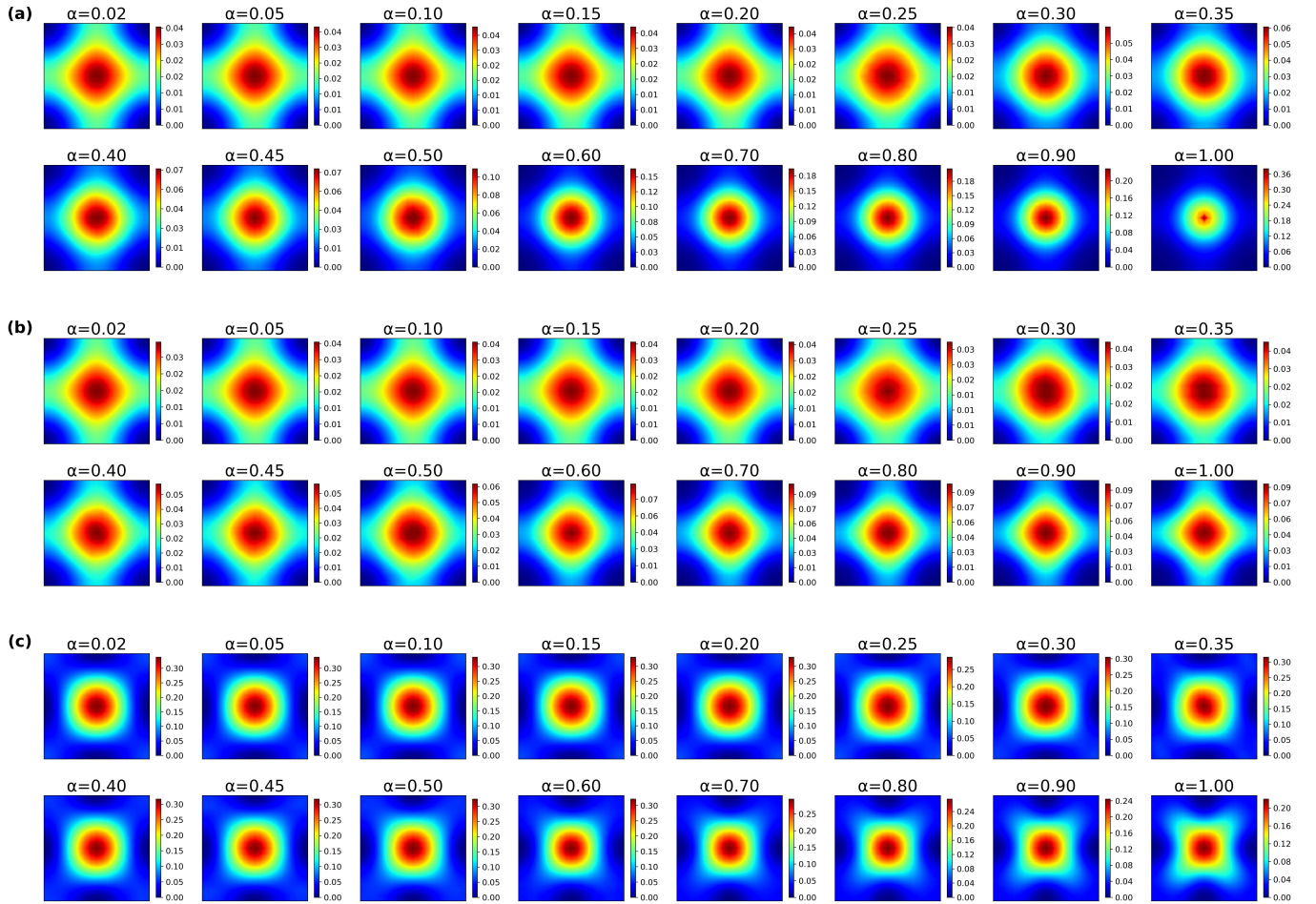


FIG. S6. (Color online) Transition of two-boson correlation by anisotropy. (a). CPQMC simulation result of s -wave boson pairing correlation $P_{s-boson}(\mathbf{k})$ from extremely anisotropy $\alpha \rightarrow 0$ to isotropic $\alpha = 1$ at $n \sim 0.63$ with $U = -3$ on 20×20 lattice. (b). CPQMC simulation result of $d_{x^2-y^2}$ -wave boson pairing correlation $P_{d_{x^2-y^2}-boson}(\mathbf{k})$ at $n \sim 0.63$. (c). CPQMC simulation result of d_{xy} -wave boson pairing correlation $P_{d_{xy}-boson}(\mathbf{k})$ at $n \sim 0.63$. They all decay to zero quickly, showing that boson correlation is short-range. The boson correlator decays much faster than the pair correlator.

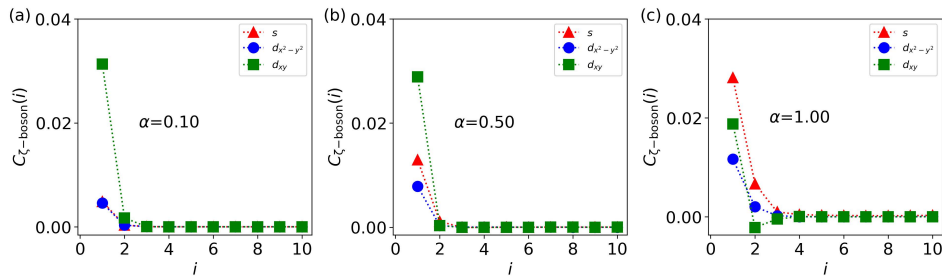


FIG. S7. (Color online) The boson pairing correlation function decay rates in real space. (a). The correlation function decay rates of different boson pairing mode $C_{z-boson}$ in real space for $\alpha = 0.10$ at $n \sim 0.63$, (b). for $\alpha = 0.50$ at $n \sim 0.63$, (c). for $\alpha = 1.00$ at $n \sim 0.63$.

S5. Constraint path quantum Monte Carlo

The CPQMC method is a quantum Monte Carlo method with a constraint path approximation [S5, S6]. In CPQMC, the ground state wave function $\psi^{(n)}$ is represented by a finite ensemble of Slater determinants, i.e., $|\psi^{(n)}\rangle \propto \sum_k |\phi_k^{(n)}\rangle$,

where k is the index of the Slater determinants, and n is the number of iteration. The overall normalization factor of the wave function has been omitted here. The propagation of the Slater determinants dominates the computational time, as follows

$$|\phi_k^{(n+1)}\rangle \leftarrow \int d\vec{x} P(\vec{x}) B(\vec{x}) |\phi_k^{(n)}\rangle. \quad (\text{S5})$$

where \vec{x} is the auxiliary-field configuration, that we select according to the probability distribution function $P(\vec{x})$. The propagation includes the matrix multiplication of the propagator $B(\vec{x})$ and $\phi_k^{(n)}$. After a series of equilibrium steps, the walkers are the Monte Carlo samples of the ground state wave function $\phi^{(0)}$ and ground-state properties can be measured.

The random walk formulation suffers from the sign problem because of the fundamental symmetry existing between the fermion ground state $|\psi_0\rangle$ and its negative $-|\psi_0\rangle$. In more general cases, walkers can cross \mathcal{N} in their propagation by $e^{-\Delta\tau H}$ whose bounding surface \mathcal{N} is defined by $\langle\psi_0|\phi\rangle = 0$ and is in general *unknown*. Once a random walker reaches \mathcal{N} , it will make no further contribution to the representation of the ground state since

$$\langle\psi_0|\phi\rangle = 0 \Rightarrow \langle\psi_0|e^{-\tau H}|\phi\rangle = 0 \quad \text{for any } \tau. \quad (\text{S6})$$

Paths that result from such a walker have equal probability of being in either half of the Slater-determinant space. Computed analytically, they would cancel, but without any knowledge of \mathcal{N} , they continue to be sampled in the random walk and become Monte Carlo noise.

The decay of the signal-to-noise ratio, i.e., the decay of the average sign of $\langle\psi_T|\phi\rangle$, occurs at an exponential rate with imaginary time. To eliminate the decay of the signal-to-noise ratio, we impose the constrained path approximation. It requires that each random walker at each step has a positive overlap with the trial wave function $|\psi_T\rangle$:

$$\langle\psi_T|\phi_k^{(n)}\rangle > 0. \quad (\text{S7})$$

This yields an approximate solution to the ground-state wave function, $|\psi_0^c\rangle = \sum_\phi |\phi\rangle$, in which all Slater determinants $|\phi\rangle$ satisfy Eq. S6. From Eq. S7, it follows that this approximation becomes exact for an exact trial wave function $|\psi_T\rangle = |\psi_0\rangle$. In Fig. S8, we find that both numerically exact DQMC and sign-constraint CPQMC gives fingerprint of CPBM (peaks in $N_{s\text{-pair}}$) in the quasi-1D lattice of two-leg ladder. This could support the applicability of using CPQMC in studying CPBM in two-dimensional lattice.

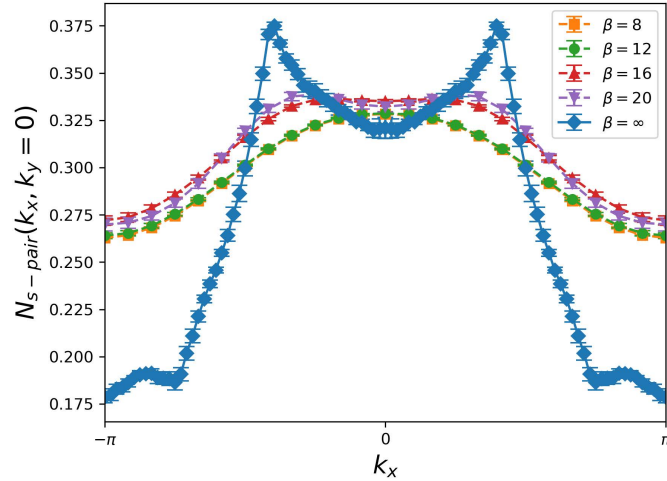


FIG. S8. (Color online) CPBM signal in two-leg ladder lattice in both CPQMC and DQMC. The divergence at pairing momentum in s -wave pair momentum distribution function $N_{s\text{-pair}}(\mathbf{k})$ of anisotropic Hamiltonian on the two-leg ladder lattice with strong anisotropy $\alpha = 0.10$ at $n \sim 0.85$ for $U = -3$. The divergence in $N_{s\text{-pair}}(\mathbf{k})$ is the fingerprint of CPBM phase in quasi-1D lattice. The blue line is the result of CPQMC in 96×2 lattice, while the other color lines are the result of determinant quantum Monte Carlo (DQMC) in 24×2 lattice, resulting the discrete momenta in $k_y = 0$ direction.

Next, we will introduce the parameter selection problem we use in the CPQMC calculation process. We choose the lattice size as 8×8 , 12×12 , 16×16 , 20×20 , so the system size N are 64, 144, 256, 400 respectively. Meanwhile,

the filling $n = (N_\uparrow + N_\downarrow)/N$, and we need to ensure that the number of \uparrow and \downarrow electrons is the same and that there cannot be a degenerate state, so n only can take some fixed values with complete shells for a lattice size. We select n is taken at intervals of 0-1 based on available complete shells, α is taken as 0.02, 0.05, 0.10, 0.15, 0.20, 0.25, 0.30, 0.35, 0.40, 0.45, 0.50, 0.60, 0.70, 0.80, 0.90, 1.00 (because the system varies more plentiful when α is small), and $U = -3$ (the most extensive region of CPBM phase). We have marked the parameter selection of n and α corresponding to different lattice size in Fig. S1(m)-(p). The details of hyper-parameters in CPQMC calculations are given as follows. The number of walkers is 1000, the number of blocks for relaxation is 10, the number of blocks for growth estimate is 3, the number of blocks after relaxation is 10, the number of steps in each block is 320, the Trotter step size is 0.02, the growth-control energy estimate is -50. The number of population control interval in relaxation phase is 10, the number of population control interval in measurement phase is 20, the number of orthonormalization interval is 10, the measurement interval is 40, the back propagation steps is 40. We provide the stability of the total energy per particles in CPQMC calculations with certain parameter changes (Fig. S9). As the lattice size increases, the computational time increases quickly, with the computational complexity dominated by the matrix multiplication. When dealing with large lattice, we design a parallelization scheme to accelerate the simulation. A convenient way to parallelize the CPQMC program is to distribute the random walkers and its associated information evenly to different cores. Three major phases are involved in the simulation, (1) relaxation, (2) growth estimation, and (3) measurement. We do parallel computing the phases of relaxation and measurement, where the majority of the computational time located. In growth estimation, the iterative update of weight leads to frequent communication between threads, and complication of parallel scheme, so we omit its parallelization.

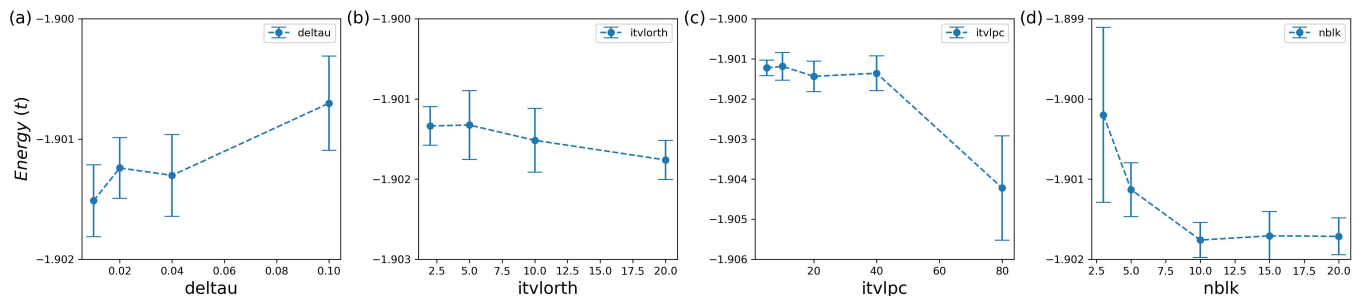


FIG. S9. (Color online) Choice of hyperparameters in CPQMC. (a-d). We show the convergence of the total energy per particles with change of hyper-parameters used in CPQMC calculations for $\alpha = 0.10$ at $U = -3$ with $n = 0.85$ on 20×20 lattice. The parameters we ultimately chose are as follows: the Trotter step size is $\text{delta tau} = 0.02$, the number of orthonormalization interval is $\text{itvlorth} = 10$, the Pop control interval in measurement phase is $\text{itvlpc} = 20$, the number of blocks for relaxation is $\text{nblk} = 10$. Some other parameters used in CPQMC calculations are provided in the method.

S6. Functional renormalization group method

The idea of FRG [S7] is to obtain the one-particle-irreducible 4-point interaction vertices Γ_{1234} (where numerical index labels single-particle state) for quasi-particles above a running infrared energy cut off Λ (which we take as the lower limit of the Matsubara frequency). Starting from $\Lambda = \infty$ where Γ is specified by on-site interaction U , the contribution to the flow (toward decreasing Λ) of the vertex is given by

$$\partial\Gamma/\partial\Lambda = -1/2P\partial\chi_{pp}/\partial\Lambda P + C\partial\chi_{ph}/\partial\Lambda C - D\partial\chi_{ph}/\partial\Lambda D \quad (\text{S8})$$

Where, P, C, D are rearrangements of Γ in the pairing(P), crossing (C) and direct(D) channels, and $\chi_{pp/ph}$ are corresponding susceptibilities in the particle-particle (PP) and particle-hole (PH) channels.

At each stage of the flow, we decompose Γ in terms of eigen scattering modes (separately) in the PP (pairing) and PH (charge density and spin density) channels in the Brillouin Zone to find the negative leading eigenvalues (NLE) S ($S < 0$), with the associated eigenfunctions describe the internal microscopic structure of the modes. The decrease of NLE S , with the flow of Λ , indicates the enhancement of fluctuation in the corresponding channel, and the divergence of which signals an emerging order at the associated scattering momentum. In the paper, we find that the dominant NLE in the PH channel is always charge density wave in the phase diagram, except the associated scattering momentum changed. However, the dominant NLE in PP channel include non-zero momentum SC and s-SF. More technical details of FRG can be found elsewhere [S8, S9].

We used two complementary numerical techniques to study the 2D system with spin-dependent anisotropy, CPQMC and FRG. While the result of CPQMC provides physical observables like correlations that is important in defining Bose metal, the result is under controllable approximation in the presence of sign problem. The FRG is a highly reliable method in term of both algorithmic foundation and the achievable lattice size, but its judgement would be based on divergence of eigenvalue on the quantity that defining known phase. In both we find consistent signals of Bose surface in CPBM phase.

-
- [S1] O. I. Motrunich and M. P. A. Fisher, *d*-wave correlated critical Bose liquids in two dimensions, [Physical review. B, Condensed matter](#) **75**, 235116 (2007).
 - [S2] A. E. Feiguin and M. P. A. Fisher, Exotic paired states with anisotropic spin-dependent Fermi surfaces, [Phys. Rev. Lett.](#) **103**, 025303 (2009).
 - [S3] A. E. Feiguin and M. P. A. Fisher, Exotic paired phases in ladders with spin-dependent hopping, [Physical review. B, Condensed matter](#) **83**, 115104 (2011).
 - [S4] H.-C. Jiang, M. S. Block, R. V. Mishmash, J. R. Garrison, D. N. Sheng, O. I. Motrunich, and M. P. A. Fisher, Non-Fermi-liquid d-wave metal phase of strongly interacting electrons, [Nature](#) **493**, 39 (2013).
 - [S5] S. Zhang, J. Carlson, and J. E. Gubernatis, Constrained path quantum Monte Carlo method for fermion ground states, [Physical review letters](#) **74**, 3652 (1995).
 - [S6] S. Zhang, J. Carlson, and J. E. Gubernatis, Constrained path Monte Carlo method for fermion ground states, [Physical review. B, Condensed matter](#) **55**, 7464 (1997).
 - [S7] C. Wetterich, Average action and the renormalization group equations, [Nuclear Physics B](#) **352**, 529 (1991).
 - [S8] W.-S. Wang, Y.-Y. Xiang, Q.-H. Wang, F. Wang, F. Yang, and D.-H. Lee, Functional renormalization group and variational Monte Carlo studies of the electronic instabilities in graphene near 1/4 doping, [Phys. Rev. B](#) **85**, 035414 (2012).
 - [S9] W.-S. Wang, C.-C. Zhang, F.-C. Zhang, and Q.-H. Wang, Theory of Chiral *p*-Wave Superconductivity with Near Nodes for Sr₂RuO₄, [Phys. Rev. Lett.](#) **122**, 027002 (2019).